

## MIT Open Access Articles

### *Air-clad silicon pedestal structures for broadband mid-infrared microphotonics*

The MIT Faculty has made this article openly available. **Please share** how this access benefits you. Your story matters.

**Citation:** Lin, Pao Tai et al. "Air-clad Silicon Pedestal Structures for Broadband Mid-infrared Microphotonics." *Optics Letters* 38.7 (2013): 1031. © 2013 Optical Society of America

**As Published:** <http://dx.doi.org/10.1364/OL.38.001031>

**Publisher:** Optical Society of America

**Persistent URL:** <http://hdl.handle.net/1721.1/79727>

**Version:** Final published version: final published article, as it appeared in a journal, conference proceedings, or other formally published context

**Terms of Use:** Article is made available in accordance with the publisher's policy and may be subject to US copyright law. Please refer to the publisher's site for terms of use.



# Air-clad silicon pedestal structures for broadband mid-infrared microphotonic

Pao Tai Lin,\* Vivek Singh, Yan Cai, Lionel C. Kimerling, and Anu Agarwal

Materials Processing Center, Massachusetts Institute of Technology, Cambridge, Massachusetts 02139, USA

\*Corresponding author: paolin@mit.edu

Received January 9, 2013; revised February 14, 2013; accepted February 15, 2013;  
posted February 21, 2013 (Doc. ID 183149); published March 20, 2013

Toward mid-infrared (mid-IR) silicon microphotonic circuits, we demonstrate broadband on-chip silicon structures, such as: (i) straight and bent waveguides and (ii) beam splitters, utilizing an air-clad pedestal configuration which eliminates the need for typical mid-IR-lossy oxide cladding. We illustrate a sophisticated fabrication process that can create high-quality pedestal structures in crystalline silicon, while preserving its mid-IR transparency. A fundamental waveguide mode is observed between  $\lambda = 2.5 \mu\text{m}$  and  $\lambda = 3.7 \mu\text{m}$ , and an optical loss of 2.7 dB/cm is obtained at  $\lambda = 3.7 \mu\text{m}$ . Our pedestal silicon structures show 50:50 mid-IR power splitting enabling the further development of mid-IR silicon microphotonic. © 2013 Optical Society of America

OCIS codes: 130.3120, 220.4000.

Mid-infrared (mid-IR) silicon photonic circuits with broad mid-IR transparency (up to  $\lambda = 8 \mu\text{m}$ ), CMOS compatibility, and robust mechanical/chemical properties [1–3], have attracted significant attention because of their potential for use in chemical sensing and environmental monitoring [4–6]. Nowadays, silicon-integrated photonics is based mainly on conventional silicon-on-insulator (SOI) technology, in which a thin layer of silicon dioxide serves as an undercladding between the top crystalline silicon waveguide and the bottom crystalline silicon substrate to prevent light leakage through the substrate. Though SOI is mature and suitable for near infrared photonic circuits, it cannot be easily adopted for planar mid-IR ( $\lambda = 3$  to  $8 \mu\text{m}$ ) devices since silicon dioxide becomes optically lossy at  $\lambda > 3.6 \mu\text{m}$  [7–9]. In the past, several approaches have been investigated to extend the application of silicon-based photonic circuits beyond  $3.6 \mu\text{m}$  [10,11]. For instance, one way is to use silicon-on-sapphire (SOS) platform instead of SOI, in which the silicon dioxide layer is replaced by sapphire, thus allowing for longer mid-IR transparency [12,13]. However, the transmittance of sapphire drops sharply at  $\lambda > 5 \mu\text{m}$  [14,15], which precludes the use of SOS devices in the chemical detection of double-bond functional groups, such as C=O, C=N, and C=C, with vibrational absorption between  $\lambda = 5 \mu\text{m}$  and  $\lambda = 8 \mu\text{m}$  [16,17]. Another platform using silicon on porous silicon was proposed for mid-IR devices, in which the waveguide cladding is a porous silicon layer created by high-energy proton beam irradiation and electrochemical etching [18]. Though low-index silicon is obtained as the undercladding, the materials damage and scattering loss caused by the high-energy irradiation has not yet been investigated. Hence, designing photonic structures or finding undercladding materials that can enable silicon as a material for broad mid-IR applications remains a challenge.

In this Letter, we demonstrate a novel air-clad silicon straight/bent waveguide and splitter, which utilizes a unique pedestal structure for broadband mid-IR devices, which is CMOS compatible and hence amenable to large-scale manufacturing. A scanning electron microscope (SEM) image confirms that device structure integrity

was maintained during fabrication processing, and broadband mid-IR transmission characterization showed a sharp fundamental waveguide mode, low mid-IR optical loss (2.7 dB/cm), and 50:50 power splitting ratio, indicating that our air-clad silicon waveguides are promising components for integrated mid-IR microphotonic.

To fabricate a pedestal silicon structure, a multistep process consisting of dry/wet etching and conformal oxide deposition is used. The detailed fabrication scheme is shown in Fig. 1. At Step (a), patterns of waveguide and beam splitter are generated on a  $3 \mu\text{m}$  thick oxide-on-silicon wafer via photolithography. At Step (b) the patterns are transferred sequentially into  $\text{SiO}_2$  and silicon with inductively coupled plasma reactive ion etching (ICP-RIE). To perform selective removals of oxide and silicon, gas mixtures composed of  $\text{H}_2/\text{CHF}_3/\text{CF}_4$  and  $\text{C}_4\text{F}_8/\text{SF}_6$  are, respectively, used to obtain etching depths of 3 and  $10 \mu\text{m}$ . At Step (c) a  $0.5 \mu\text{m}$  thick oxide layer is conformally deposited on the sample using plasma-enhanced chemical vapor deposition (PECVD). At Step (d) the conformally deposited oxide is etched back anisotropically in certain areas using ICP-RIE, removing only part of the oxide as shown in Fig. 1(d). In other words, a thin oxide is intentionally left on the sidewall of the waveguide to protect its surface. In Step (e), undercut of waveguide is performed by isotropic silicon etching using  $\text{SF}_6$  gas. Only the surface without an oxide covering is removed. Afterward, a narrow strip is revealed below the silicon waveguide that supports the upper mid-IR planar structure. In Step (f), once the desired pedestal silicon structure is obtained, the remaining oxide is removed by buffered oxide etch (BOE). The structure parameters that are used to define the pedestal configuration are waveguide width  $w$ , waveguide height  $h$ , lift-off length  $s$ , and the notch width  $d$ . These four parameters determine the waveguide performance, and they can be modified by changing the associated pattern design or by alternative etching methods.

The fabricated mid-IR waveguides and beam splitters were inspected by SEM and the images are shown in Fig. 2. The sample is tilted at  $54^\circ$  during microscopy to improve the cross-sectional images. From Fig. 2(a) and the magnified image in Fig. 2(b), we see that the

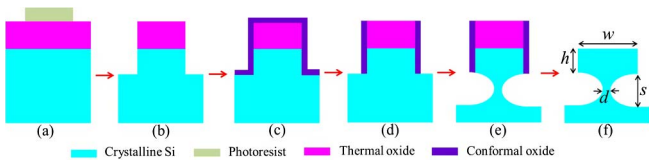


Fig. 1. (Color online) Fabrication scheme to create pedestal silicon waveguides and splitters. (a) Patterns of waveguide and splitter are generated on oxide-on-silicon wafer by photolithography. (b) Patterns are transferred sequentially into SiO<sub>2</sub> and Si layers using ICP-RIE. (c) A thin oxide layer is conformally deposited on the sample using PECVD. (d) Oxide is anisotropically and preferentially etched back using ICP-RIE. (e) Undercut of silicon waveguide using SF<sub>6</sub> gas. (f) Oxide is removed by BOE. The structure parameters, waveguide width  $w$ , waveguide height  $h$ , lift-off length  $s$ , and the notch width  $d$ , are labeled.

waveguide edges (top of the structure) are smooth (no bumps or indentations are found); also the waveguide edges remain straight (no bending or distortion is observed); and finally the waveguide structure is well resolved (no cracks or roughness is seen on the waveguide edges). This indicates that silicon pedestal structures are successfully created by the fabrication process described in Fig. 1. Meanwhile, from the magnified image the structure parameters are obtained as  $w = 8 \mu\text{m}$ ,  $h = 5 \mu\text{m}$ ,  $s = 14 \mu\text{m}$ , and  $d = 2 \mu\text{m}$ , in keeping with the original design. The sample is then rotated by 45° to visualize the morphology of the waveguide sidewalls and shown in Fig. 2(c) and enlarged in 2(d). No defects are found in the vertical facets, confirming that the conformally deposited oxide layer did effectively protect the waveguide cores during the isotropic silicon etching. Figure 2(e) is the image of an individual waveguide that has a paper clip shape, and its radius of the curvature is 50  $\mu\text{m}$ . Clearly the suspended bent waveguide is well supported by the strip underneath. To prove that our novel fabrication methods are capable of generating useful mid-IR circuits, we demonstrate pedestal beam splitters that can efficiently separate light into several output ports. As shows in Fig. 2(f), an array of well-defined Y-branch splitters is accomplished. The magnified image reveals a highly symmetric structure, which is a critical first step to achieving a 50:50 power splitting ratio.

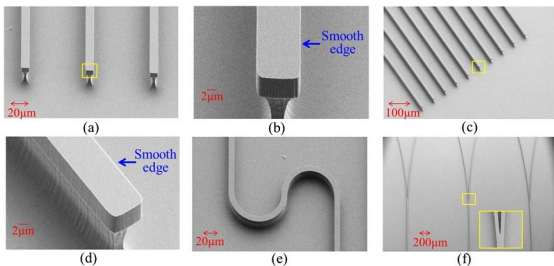


Fig. 2. (Color online) SEM images of the fabricated air-clad silicon pedestal mid-IR devices: (a) Straight waveguides, (b) magnified image, (c) rotated at 45° to inspect the waveguide sidewall, (d) enlarged image, (e) waveguide that has a paper clip shape with a radius of curvature of 50  $\mu\text{m}$ , and (f) Y-branch beam splitters. The yellow boxes indicate the magnified features.

The mode profiles of the silicon pedestal waveguides are numerically simulated to optimize its light-guiding performance in the mid-IR spectral range. The simulation method used is two dimensional finite difference method (FDM) calculations. Figure 3(a) illustrates the pedestal configuration used in the modeling. The structure parameters are  $w = 8 \mu\text{m}$ ,  $h = 5 \mu\text{m}$ ,  $s = 14 \mu\text{m}$ , and  $d = 2 \mu\text{m}$ , which match the device dimensions experimentally observed from the SEM characterization. A light source of  $9 \mu\text{m} \times 9 \mu\text{m}$  is chosen so its size is comparable to the experimental one, a single-mode fiber with 9  $\mu\text{m}$  core diameter. The field profiles of the air-clad waveguide mode are calculated at  $\lambda = 2.7 \mu\text{m}$ ,  $\lambda = 3.2 \mu\text{m}$ , and  $\lambda = 3.7 \mu\text{m}$ , and depicted in Fig. 3. A fundamental mode is clearly resolved where the lightwave is highly confined inside the upper silicon waveguide. In addition, negligible variation is observed in the mode profiles when the wavelength is scanned over a broad spectral range.

To experimentally evaluate the performance of the fabricated silicon waveguides and splitters, we set up a mid-IR test platform as illustrated in Fig. 4(a). The light source is a pulsed laser with 150 mW average power and the laser wavelength is tunable from  $\lambda = 2.4 \mu\text{m}$  to  $\lambda = 3.7 \mu\text{m}$ . Using a reflective lens, the probe light is first collimated into a 9  $\mu\text{m}$  core and 125  $\mu\text{m}$  cladding fluoride fiber, and then butt coupled into the waveguide. As shown in Fig. 4(b), the core of the mid-IR fiber is lined up with the smooth cleaved front facet of the silicon waveguide. Alignment between the optical fiber and the waveguide is achieved using high-precision positioning stages and the fine adjustment is monitored by an upper microscope equipped with a long working distance objective. The mid-IR signals from the waveguides are focused by a calcium fluoride biconvex lens and then imaged by a InSb camera.

The waveguide modes of the pedestal silicon waveguides are characterized from 2.5 to 3.7  $\mu\text{m}$ , where the mode profiles at  $\lambda = 2.7 \mu\text{m}$ ,  $\lambda = 3.2 \mu\text{m}$ , and  $\lambda = 3.7 \mu\text{m}$  are captured by the mid-IR camera and depicted

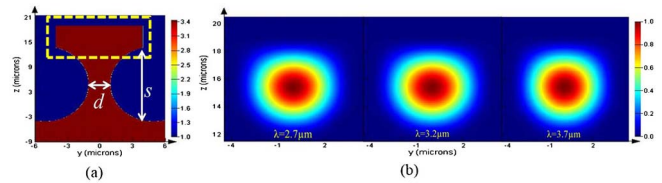


Fig. 3. (Color online) (a) Refractive index profile of pedestal structure used for the FDM mode calculation. The yellow box indicates the light source. (b) The field profiles of the waveguide at  $\lambda = 2.7 \mu\text{m}$ ,  $\lambda = 3.2 \mu\text{m}$  and  $\lambda = 3.7 \mu\text{m}$ .

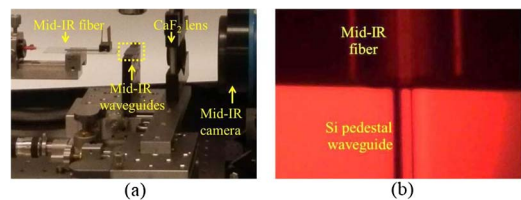


Fig. 4. (Color online) (a) Experimental setup to characterize the performance of fabricated mid-IR devices. (b) The probe light is butt coupled into the waveguide from a single-mode fluoride fiber.

in Fig. 5(a). From the images, a sharp fundamental mode is clearly resolved as predicted by the FDM simulation. No scattering or distortion is shown, which implies that the mid-IR probe light is well confined inside the pedestal Si waveguides. Furthermore, the fundamental mode remains the dominant one within the wide spectral range, indicating that the air-clad waveguides can efficiently deliver broadband mid-IR signals on-chip. To characterize the optical loss, we measure the attenuation of optical powers from waveguides that have similar paper clip shape but with different lengths. As shown in Fig. 5(b), the paper clip center distance  $D$  varies from 1 to 4 mm and matches a change of waveguide length from 2 to 8 mm. By fitting the length-dependent optical powers from the waveguide outputs, an optical loss of as low as 2.7 dB/cm is obtained at  $\lambda = 3.7 \mu\text{m}$  with an measurement error less than 0.15 dB/cm. Overall, using the pedestal structure, we are able to utilize the air-cladding for efficient wave guiding compared to a mid-IR lossy oxide cladding which is known to have considerable attenuation at  $\lambda > 3.6 \mu\text{m}$ .

The performance of the  $Y$ -branch splitters supported by a pedestal structure is also evaluated. Figure 6(a) is the image from the splitter outputs at  $\lambda = 3.2 \mu\text{m}$ , showing two sharp spots arising, respectively, from a fundamental mode from each arm of the waveguide splitter. Clearly there is no higher-order mode excited when the lightwave is passing through the input single-arm into the output double-arms. The intensity profile across the  $x$  axis is measured to characterize the power splitting ratio. As shown in Fig. 6(b), two peaks that have identical maximum intensities are found. The success of making a high-quality beam splitter enables the distribution of lightwaves into multiple waveguide channels and consequently paves the way for making sophisticated mid-IR planar array devices.

In conclusion, we design and fabricate broadband silicon mid-IR circuits utilizing a unique pedestal structure. The lightwave confinement is accomplished by using an air-clad structure instead of mid-IR lossy oxide, to enable low-loss transmission beyond  $\lambda = 3.6 \mu\text{m}$ . We demonstrate that our fabrication process can generate various planar mid-IR structures, including straight/curved waveguides and beam splitters. No distortion or damage is found on the waveguide sidewalls even after a multistep dry/wet etching process. A fundamental mode is experimentally observed between  $\lambda = 2.5 \mu\text{m}$  and  $\lambda = 3.7 \mu\text{m}$  and the result agrees well with the FDM simulation. An optical loss of 2.7 dB/cm is obtained at  $\lambda = 3.7 \mu\text{m}$ .

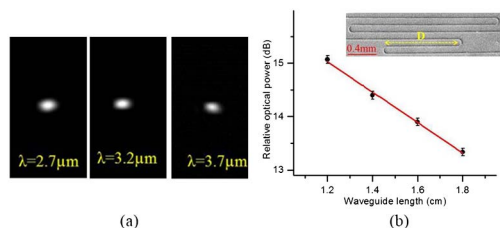


Fig. 5. (Color online) (a) Mode profiles of pedestal silicon waveguides captured by the mid-IR camera at  $\lambda = 2.7 \mu\text{m}$ ,  $\lambda = 3.2 \mu\text{m}$ , and  $\lambda = 3.7 \mu\text{m}$ . (b) Optical powers from waveguides with different relative length  $D$ . By fitting the data, an optical loss of 2.7 dB/cm is obtained at  $\lambda = 3.7 \mu\text{m}$ .

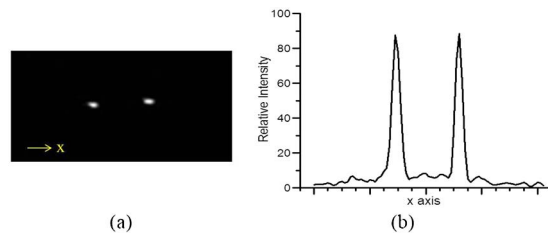


Fig. 6. (Color online) (a) Mid-IR image from a  $Y$ -branch waveguide splitter at  $\lambda = 3.2 \mu\text{m}$ . (b) The intensity profile across the  $x$  axis shows two peaks with identical maximum intensities.

In addition, we show waveguide splitters using the pedestal structure can reach a desired 50:50 splitting ratio. Our results provide a method of utilizing silicon for mid-IR planar devices up to  $\lambda = 3.7 \mu\text{m}$ .

Device fabrication was performed at the Microsystems Technology Laboratories and Center for Materials Science and Engineering at MIT, and the Center for Nanoscale Systems at Harvard University. Optical calculation was assisted by the Center for Nanoscale Materials in Argonne National Laboratory.

## References

- X. Liu, R. M. Osgood, Jr., Y. A. Vlasov, and W. M. J. Green, *Nat. Photonics* **4**, 557 (2010).
- R. Shankar, R. Leijssen, I. Bulu, and M. Lončar, *Opt. Express* **19**, 5579 (2011).
- R. K. W. Lau, M. Ménard, Y. Okawachi, M. A. Foster, A. C. Turner-Foster, R. Salem, M. Lipson, and A. L. Gaeta, *Opt. Lett.* **36**, 1263 (2011).
- X. Fan and I. M. White, *Nat. Photonics* **5**, 591 (2011).
- J. Ozhikandathil and M. Packirisamy, *J. Biomed. Opt.* **17**, 017006 (2006).
- K. Reddy, Y. Guo, J. Liu, W. Lee, M. K. Khaing, and X. Fan, *Lab On Chip* **12**, 901 (2012).
- P. Y. Yang, S. Stankovic, J. Crnjanski, E. J. Teo, D. Thomson, A. A. Bettiol, M. B. H. Breese, W. Headley, C. Giusca, G. T. Reed, and G. Z. Mashanovich, *J. Mater. Sci. Mater. Electron.* **20**, 159 (2009).
- G. Z. Mashanovich, M. M. Milošević, M. Nedeljkovic, N. Owens, B. Xiong, E. J. Teo, and Y. Hu, *Opt. Express* **19**, 7112 (2011).
- R. Soref, *Nat. Photonics* **4**, 495 (2010).
- Y. Wei, G. Li, Y. Hao, Y. Li, J. Yang, M. Wang, and X. Jiang, *Opt. Express* **19**, 15803 (2011).
- Z. Cheng, X. Chen, C. Y. Wong, K. Xu, C. K. Y. Fung, Y. M. Chen, and H. K. Tsang, *IEEE Photon. J.* **4**, 104 (2012).
- T. Baehr-Jones, A. Spott, R. Ilic, A. Spott, B. Penkov, W. Asher, and M. Hochberg, *Opt. Express* **18**, 12127 (2010).
- F. Li, S. D. Jackson, C. Grillet, E. Magi, D. Hudson, S. J. Madden, Y. Moghe, C. O'Brien, A. Read, S. G. Duvall, P. Atanackovic, B. J. Eggleton, and D. J. Moss, *Opt. Express* **19**, 15212 (2011).
- E. D. Palik, *Handbook of Optical Constants of Solids* (Academic, 1997).
- D. A. Gryvnak and Darrell E. Burch, *J. Opt. Soc. Am.* **55**, 625 (1965).
- H. Gunzler and H. U. Gremlich, *IR Spectroscopy: An Introduction* (Wiley-VCH, 2002).
- R. M. Silverstein, F. X. Webster, and D. Kiemle, *Spectrometric Identification of Organic Compounds* (Wiley, 2005).
- G. Z. Mashanovich, M. M. Milošević, M. Nedeljkovic, N. Owens, B. Xiong, E. J. Teo, and Y. Hu, *Opt. Express* **19**, 7112 (2011).